ISSN 1063-7761, Journal of Experimental and Theoretical Physics, 2018, Vol. 126, No. 1, pp. 21–34. © Pleiades Publishing, Inc., 2018.
Original Russian Text © A.G. Litvak, V.A. Mironov, S.A. Skobelev, L.A. Smirnov, 2018, published in Zhurnal Eksperimental'noi i Teoreticheskoi Fiziki, 2018, Vol. 153, No. 1, pp. 28–44.

ATOMS, MOLECULES, OPTICS

Peculiarities of the Self-Action of Inclined Wave Beams Incident on a Discrete System of Optical Fibers

A. G. Litvak[a], V. A. Mironov[a], S. A. Skobelev[a,*], and L. A. Smirnov[a, b,]**

[a] *Institute of Applied Physics, Russian Academy of Sciences, Nizhny Novgorod, 603950 Russia*

[b] *Lobachevskii Nizhny Novgorod State University, Institute of Information Technologies, Mathematics and Mechanics, Nizhny Novgorod, 603950 Russia*

** e-mail: sksa@ufp.appl.sci-nnov.ru*

*** e-mail: smirnov_lev@appl.sci-nnov.ru*

Received July 30, 2017

Abstract—Based on a discrete nonlinear Schrödinger equation (DNSE), we studied analytically and numerically the peculiarities of the self-action of one-dimensional quasi-optic wave beams injected into a spatially inhomogeneous medium consisting of a set of equidistant mutually coupled optical fibers. A variational approach allowing the prediction of the global evolution of localized fields with the initially plane phase front was developed. The self-consistent equations are obtained for the main parameters of such beams (the position of the center of mass, the effective width, and linear and quadratic phase-front corrections) in the aberrationless approximation. The case of radiation incident on a periodic system of nonlinear optical fibers at an angle to the axis oriented along them is analyzed in detail. It is shown that for the radiation power exceeding a critical value, the self-focusing of the wave field is observed, which is accompanied by the shift of the intensity maximum followed by the concentration of the main part of radiation only in one of the structural elements of the array under study. In this case, the beams propagate along paths considerably different from linear and the direction of their propagation changes compared to the initial direction. Asymptotic expressions are found that allow us to estimate the self-focusing length and to determine quite accurately the final position of a point with the maximum field amplitude after radiation trapping a channel. The results of the qualitative study of the possible self-channeling regimes for wave beams in a system of weakly coupled optical fibers in the aberrationless approximation are compared with the results of direct numerical simulations within the DNSE framework.

DOI: 10.1134/S1063776118010053

1. INTRODUCTION

One of the basic models for studying the self-action of wave fields in a continuous medium is the nonlinear Schrödinger equation (NSE) playing an important role in optics, plasma physics, hydrodynamics, and in the field of ultracold degenerate quantum gases [1–3]. This model (and its modifications) was used to develop a variety of analytic methods explaining the key features in the behavior of one or several mutually interacting localized systems with finite amplitudes. Methods of the qualitative analysis of the problem such as, for example, the construction of self-similar and soliton-like solutions, the method of moments, the asymptotic expansion in a small parameter, the variational approach, etc. [1–3], allow one to not only interpret but also predict the results of numerical calculations and laboratory experiments.

Nonlinear processes in periodic structured systems are often studied using the discrete nonlinear Schrödinger equation (DNSE) [2–9], which is a direct analog of the NSE for spatially stratified media. However, in this case, the evolution of wave fields is analyzed, as a rule, based on numerical simulations [2–9]. This is explained, first of all, by the fact that the application of standard asymptotic procedures becomes more complicated and quite cumbersome. In addition, a combination of nonlinearity and discreteness gives rise to new physical effects, in particular, related to drastic structural changes of localized systems and considerable radiative losses. As a result, the system dynamics proves to be more complicated [2–10], and discrete models, even in the one-dimensional case, demonstrate a number of scenarios of their behavior that are not encountered in the continual limit and require a separate analytic description and understanding. For this purpose, a variational approach is often used that is based on a priori concepts about the structure of nonlinear excitations under study [1–4, 9, 10]. In particular, this approach for the DNSE was used to estimate the amplitude and width of stationary soliton-like distributions [11–19].

The variational method can also be quite effective for the qualitative study of the evolution of localized systems [18–22].

In this work, we studied analytically and numerically within the DNSE framework the features of the self-action of intense wave fields. For definiteness, processes under study are considered by the example of Gaussian optical beams injected at an angle to a spatially inhomogeneous medium consisting of equidistantly arranges optical fibers. Interest in this problem is explained first of all by the fact that light beams in modern fiber optics are controlled with the help of periodic waveguides [3–8, 23, 24]. The theoretical description of various aspects of the evolution of laser radiation presented below can be used for interpretation and prediction of variations in the propagation direction of the electromagnetic field and its self-channeling in one of the structural elements of these systems. Note that such effects have been already observed directly in experiments [25–29]. Note also that, due to the universality of the DNSE model, the results presented here can be also applied in other fields of physics [2–9], in particular, in the dynamics of the Bose–Einstein condensate in optical lattices [20, 30–34].

This paper is organized as follows. In Section 2, the variational approach is developed for describing the key features of radiation evolution in a periodic structural medium. Here, using this method, we obtained in Section 2.1 a closed self-consistent system of equations for the position of the center and the effective width of the amplitude profile and linear and quadratic corrections of the phase front of a quasi-optical Gaussian beam. In Section 2.2, these truncated equations were used for the qualitative analysis of the self-action regimes of the wave field in an array of weakly coupled optical fibers. In Section 3, we present the results of direct numerical simulations within the DNSE framework and compare them with the analytic study of the spatial beam dynamics. A special attention is devoted to radiative losses during radiation self-channeling in one of the nonlinear optical fibers. In Conclusions (Section 4), the main results of the paper are formulated. In Appendix A, we discuss modifications caused by consideration of additional terms in the variational procedure that were neglected in Section 2.1. In Appendix B, we analyze in detail the possible scenarios of behavior of a wave beam in an array of optical fibers based on the phase plane of a system of ordinary differential equations for the effective width of the amplitude distribution and the phase front curvature.

2. ANALYTIC DESCRIPTION OF THE EVOLUTION OF WAVE BEAMS IN AN ARRAY OF OPTICAL FIBERS

2.1. Variational Approach to a Problem of Radiation Self-Focusing in a Discrete Medium

Consider the features of the self-action of one-dimensional quasi-optical wave beams injected into a spatially inhomogeneous medium consisting of an infinite number of equidistantly arranged single-mode delta-shaped optical fibers with the Kerr (cubic) nonlinearity. In an ideal system (in the absence of losses), we arrive at an infinite ordered sequence of relations, which is called the DNSE and has the form [3–8]

$$i\frac{\partial \Psi_n}{\partial z} + \Psi_{n-1} + \Psi_{n+1} + |\Psi_n|^2\Psi_n = 0 \qquad (1)$$

in normalized variables. Here, the function $\Psi_n(z)$ determines the complex amplitude of the mode of the nth directing element oriented parallel to the z axis of an array of weakly coupled optical waveguides in which dispersion and diffraction effects can be neglected. DNSE model (1) is one of the simplest and universal discrete models. As its continuous NSE analog, this model has the Hamiltonian structure and two integrals of motion [2–8]

$$\mathcal{P} = \sum_{n=-\infty}^{+\infty} |\Psi_n|^2, \qquad (2)$$

$$\mathcal{H} = \sum_{n=-\infty}^{+\infty} \left(\Psi_{n+1}^* \Psi_n + \text{c.c.} + \frac{1}{2}|\Psi_n|^4 \right). \qquad (3)$$

Preserving quantities $\mathcal{P}$ and $\mathcal{H}$ are directly connected with the beam power and energy in the problem under study [2–8]. In fact, $\mathcal{P}$ is a controlling parameter whose value considerably determines the radiation propagation process, while expression (3) is the Hamiltonian of model (1).

Using (1), we analyzed in detail the possible scenarios of propagation of an initially collimated wave beam coupled into a periodic system of optical fibers at an angle to the z axis oriented along them. For this purpose, we used the variational approach, which is quite universal and is often applied for the analytic study of the dynamics and interaction of localized systems in various nonlinear media [1–5, 9, 10].

First, using the Poisson summation formula (for example, see [20–22]), we rewrite the Lagrange function corresponding to DNSE (1) [2–5, 11–19] in the form

$$\mathcal{L} = \sum_{n=-\infty}^{+\infty} \frac{i}{2}\left(\Psi_n \frac{\partial \Psi_n^*}{\partial z} + \text{c.c.}\right) - \mathcal{H}$$
$$= \int_{-\infty}^{+\infty} \left(\frac{i}{2}\Psi(x,z)\frac{\partial \Psi^*(x,z)}{\partial z} - \Psi^*(x+1,z)\right. \quad (4)$$
$$\left.\times \Psi(x,z) - \text{c.c.} - \frac{1}{2}|\Psi(x,z)|^4\right) \sum_{n=-\infty}^{+\infty} e^{2\pi i n x} dx.$$

This allows us to work with the only function $\Psi(x, z)$ instead of an infinite ordered set of complex amplitudes $\Psi_n(z)$ in each of the waveguides. This function depends now not only on the coordinate z, but also on a continuous argument x.

Then, we assume that the radiation intensity distribution is described by a Gaussian with the effective width $a(z)$ and the center at the point $x_0(z)$, while the phase front contains only linear and quadratic corrections with the corresponding coefficients $\gamma(z)$ and $\beta(z)$. In other words, we approximate $\Psi(x, z)$ by the expression

$$\Psi(z,x) = \sqrt{\frac{\mathcal{P}}{\sqrt{\pi}a}}$$
$$\times \exp\left(-\frac{(x-x_0)^2}{2a^2} + i\gamma(x-x_0) + i\beta(x-x_0)^2\right), \quad (5)$$

corresponding to the aberrationless approximation [2, 3].

By substituting (5) into (4) and integrating over the continuous variable x, we obtain a functional series with coefficients decreasing exponentially with increasing n (for example, [20–22]). It follows directly from the structure of this series that for the condition $a(z) \gg \sqrt{2}/\pi$, i.e., even for wave fields with the characteristic transverse size $a(z)$ comparable with the period of the array of optical fibers, self-action processes can be approximately analytically described by keeping only the term with $n = 0$ in (4).

As a result, we obtain the averaged Lagrange function $\overline{\mathcal{L}}$ of the system under consideration in the form

$$\overline{\mathcal{L}} = \frac{\mathcal{P}a^2}{2}\frac{d\beta}{dz} - \mathcal{P}\gamma\frac{dx_0}{dz}$$
$$-2\mathcal{P}\cos\gamma\exp\left(-\frac{1}{4a^2} - \beta^2 a^2\right) - \frac{\mathcal{P}^2}{\sqrt{8\pi}a}. \quad (6)$$

The Euler equation for collective coordinates $a(z)$, $\beta(z)$, $x_0(z)$, and $\gamma(z)$ corresponding to the truncated Lagrangian $\overline{\mathcal{L}}$ (6) takes the form

$$\frac{da}{dz} = 4\beta a\cos\gamma\exp\left(-\frac{1}{4a^2} - \beta^2 a^2\right), \quad (7a)$$

$$\frac{d\beta}{dz} = \frac{\cos\gamma}{a^2}\left(\frac{1}{a^2} - 4\beta^2 a^2\right)$$
$$\times\exp\left(-\frac{1}{4a^2} - \beta^2 a^2\right) - \frac{\mathcal{P}}{\sqrt{8\pi}a^3}, \quad (7b)$$

$$\frac{dx_0}{dz} = 2\sin\gamma\exp\left(-\frac{1}{4a^2} - \beta^2 a^2\right), \quad (7c)$$

$$\frac{d\gamma}{dz} = 0. \quad (7d)$$

These relations clearly demonstrate that the beam evolution in discrete model (1) significantly differs from its spatial dynamics in the continual situation described by the NSE and proceeds over complicated scenarios. In particular, according to (7c), the displacement of the radiation intensity maximum $x_0(z)$ across the optical fiber array depends on the effective width $a(z)$ and the curvature $\beta(z)$ of the phase front of the wave field. The passage to the limit from Eqs. (7a)–(7d) to their analogs in the continuous case proves to be rather nontrivial, because it is necessary to assume not only that $a \gg 1$, but also that $\beta a \ll 1$. It is when these two conditions are simultaneously fulfilled in the paraxial approximation ($\gamma \ll 1$), we arrive instead of (7c) at the result $dx_0/dz = 2\gamma$ well known for a continuous medium.

Note that within the framework of variational description developed in this section, taking into account only the term with $n = 0$ in Lagrangian (4), the coefficient γ responsible for the linear correction of the wave-field phase front, according to (7d), is independent of the coordinate z and remains equal to its initial value γ_0 along the entire radiation propagation path, i.e., $\gamma = \gamma_0$. Therefore, by analyzing the behavior of beams with the help of self-consistent Eqs. (7a)– (7b), we will use γ_0 instead of γ. It should be emphasized that, if the averaged Lagrangian $\overline{\mathcal{L}}$ is calculated taking into account not only the terms of the series with $n = 0$ but also with $n = \pm 1$, then the derivative $d\gamma/dz$ will become nonzero and the value of γ will change with increasing z even within the framework of the aberrationless approximation (see Appendix A). However, these effects do not strongly affect processes discussed in the paper and can be neglected for simplifying further calculations and estimating critical values of parameters of the problem.

2.2. Self-Channeling Regime. Change in the Beam Propagation Direction Due to Radiation Self-Focusing

Consider the wave-field focusing in discrete model (1) based on the self-consistent system of equations (7a)–(7d) for the main parameters of Gaussian beam (5) in the aberrationless approximation. According to (7a)–(7d), the shift of the radiation intensity maximum $x_0(z)$ across the z axis does not affect the spatial dynamics of the effective with $a(z)$ of the amplitude distribution and the phase-front curvature $\beta(z)$. In turn, the propagation path of the wave field as a whole strongly depends on the behavior of $a(z)$ and $\beta(z)$ and is determined by relation (7c). Under these conditions, it is reasonable to divide analysis into two

stages. At the first stage for $\gamma = \gamma_0$, a system of autonomous ordinary differential equations (7a), (7b) and its possible solutions are considered, and at the second stage, their influence on the change in $x_0(z)$ is discussed based on expression (7c).

By the change of variables $\zeta = z\cos\gamma_0$, relations (7a) and (7b) can be reduced to the form in which the only parameter

$$Q = \mathcal{P}/\sqrt{8\pi}\cos\gamma_0 \tag{8}$$

is present. This means that the evolution of the beam internal structure depends first of all on the value of Q directly related to the power $\mathcal{P}$. In addition, Eqs. (7a) and (7b) are Hamiltonian equations in canonic variables a^2 and β, which follows from the presence of the Hamiltonian (3) for DNSE (1). Thus, the dynamic system (7a), (7b) has the first integral of motion, which we present for convenience in the form

$$\mathcal{C} = \exp\left(-\frac{1}{4a^2} - \beta^2 a^2\right) + \frac{Q}{2a}. \tag{9}$$

The conservation law (9) allows one to analyze the a, β phase plane for different Q (see Appendix B), thereby providing the advance in the analytic solution of the problem and revealing the conditions under which critical changes in the beam propagation process should be expected.

The study (see details in Appendix B) of the features of the phase space of the system of equations (7a), (7b) taking (9) into account shows that there exist two critical powers $\mathcal{P}'_{cr}$ and $\mathcal{P}_{cr}$ connected with bifurcation values $Q'_{cr} \approx 0.638$ and $Q_{cr} = \sqrt{2/e} \approx 0.858$ by the relations

$$\mathcal{P}'_{cr} = \sqrt{8\pi}Q'_{cr}\cos\gamma_0 \approx 1.276\sqrt{2\pi}\cos\gamma_0, \tag{10}$$

$$\mathcal{P}_{cr} = \sqrt{8\pi}Q_{cr}\cos\gamma_0 = 4\sqrt{\pi/e}\cos\gamma_0. \tag{11}$$

If the radiation power $\mathcal{P}$ falls into the interval $0 < \mathcal{P} \le \mathcal{P}'_{cr}$, the situation is qualitatively the same as in a continuous medium described by the NSE. In this case, the transverse size $a(z)$ of the initial collimated beam with $a(z = 0) = a_0$ will either increase infinitely or oscillate along the propagation path. In this case, the field will be never captured in one optical fiber. When $\mathcal{P} \ge \mathcal{P}_{cr}$, in contrast, radiation will be always collected in a channel with the characteristic scale

$$a_{ch} = Q/2\mathcal{C} = \mathcal{P}/(4\sqrt{2\pi}\mathcal{C}\cos\gamma_0), \tag{12}$$

which is determined by the value of $\mathcal{P}$ and the first integral (9) of problem (7a), (7b). Note, however, that for the above considerations to be valid, $\mathcal{P}$ should not exceed $\mathcal{P}_{cr}$ too strongly, because otherwise the approximation of the field amplitude distribution by a Gaussian is quite rapidly violated with increasing z. In the intermediate case, when $\mathcal{P}'_{cr} < \mathcal{P} < \mathcal{P}_{cr}$, the effective width $a(z)$ of the wave beam with the initially plane phase front, depending on its start value a ($z = 0$) $= a_0$, can either change periodically or collapse during self-focusing, becoming on the order of the lattice period. Therefore, the real critical power $\mathcal{P}_{cr1}$ above which radiation self-channeling is observed is not a universal quantity, but is determined by a_0. The form of the function $\mathcal{P}_{cr1}(a_0)$ can be found from analytic results described in Appendix B. In particular, it follows from them that $\mathcal{P}_{cr1}(a_0)$ monotonically decreases from $\mathcal{P}_{cr}$ to $\mathcal{P}'_{cr}$ with increasing a_0.

Let us estimate the characteristic self-focusing length. Consider the situation when the wave beam with initially plane phase front is wide enough, i.e., $\beta(z = 0) = 0$, $a(z = 0) = a_0 \gg 1$, and the radiation power $\mathcal{P}$ exceeds $\mathcal{P}_{cr1}(a_0)$. Until the field collected in a channel, we can assume (at least at the first stage of radiation propagation) that the effective beam width $a(z)$ is comparatively large, i.e., $a \gg 1$ (however, $a(z) \lesssim a_0$), which allows us to separate a small parameter $\varepsilon \sim 1/a$ in the problem. Using relation (9), we represent the product $\beta^2 a^2$ as a function of a, which will be expanded into an asymptotic series in ε. Retaining in this expansion only the main terms on the order of ε and taking in to account that $\mathcal{C} \approx 1 + Q/2a_0$, we obtain the approximation

$$\beta = \pm\sqrt{Q(a_0 - a)/2a_0a^3} \tag{13}$$

for the dependence of the phase-front curvature $\beta(z)$ on the size $a(z)$ of the amplitude distribution. By substituting (13) into (7a), we finally arrive at the simplified equation for $a(z)$,

$$\frac{da}{dz} = \pm 4\sqrt{\frac{Q(a_0 - a)}{2a_0a}}\cos\gamma_0. \tag{14}$$

Its solution specifies $a(z)$ in the form of the implicit function

$$-\sqrt{a(a_0 - a)} - a_0\left(\frac{\pi}{2} - \arcsin\sqrt{\frac{a}{a_0}}\right) = \pm 4\sqrt{\frac{Q}{2a_0}}z\cos\gamma_0. \tag{15}$$

Note that the sign "+" in relations (13), (14), and (15) corresponds to negative values of z. In this case, the phase-front curvature $\beta(z)$ of the wave field is positive and the effective width $a(z)$ increases with approaching z to zero, achieving its maximum a_0 for $z = 0$. The choice of the sign "–" in relations (13), (14), and (15) corresponds to the situation when radiation propagates in the region $z > 0$. Here, the transverse size $a(z)$ of the beam, on the contrary, decreases with increasing z and $\beta(z) < 0$.

Figure 1a demonstrates a comparison between the implicit approximation (15) for the function $a(z)$ and direct calculations performed using Eqs. (7a)–(7d).

One can see that expression (15) adequately reproduces the behavior of the effective width $a(z)$ of the beam in the aberrationless approximation, not only for $a \gg 1$, but also for a, comparable with the lattice period.

According to (15), $a(z)$ should vanish at the point $z = z_0$, where

$$z_0 = \frac{\pi a_0^{3/2}}{4\sqrt{2Q}\cos\gamma_0} = \frac{\pi^{5/4} a_0^{3/2}}{2^{7/4}\sqrt{\mathcal{P}\cos\gamma_0}}, \qquad (16)$$

approaching zero by the law $\propto (z_0 - z)^{2/3}$. Note that z_0 decreases inversely proportional to $\sqrt{\mathcal{P}\cos\gamma_0}$. In reality, beginning from z close to z_0, $a(z)$ tends to a stationary value a_{ch} and a channel is formed gradually. The distance z_0 can be used as the estimate of the self-focusing length as long as $a_{ch} \lesssim 1$, i.e., for the power $\mathcal{P}$ not strongly exceeding the critical value $\mathcal{P}_{cr}$, as follows from (12). A more accurate estimate can be obtained from expression (15), where a is replaced by a_{ch}, determined by expression (12).

At the final stage of the radiation self-channeling process, the discreteness of the system under study begins to play a key role, which substantially affects the evolution of the main parameters of the wave beam. In particular, assuming in (7a) and (7b) that the effective width $a(z)$ of the field amplitude distribution approaches a_{ch} with increasing z, while, on the contrary, the phase front curvature $\beta(z)$ increases infinitely, we find the behavior of $a(z)$ and $\beta(z)$ for $z \to \infty$:

$$a(z) \approx a_{ch} + \frac{2a_{ch}^2}{Q}\exp\left(-\frac{1}{4a_{ch}^2} - \frac{\mathcal{P}^2}{8\pi a_{ch}^4}(z - z_1)^2\right), \qquad (17)$$

$$\beta(z) \approx -\mathcal{P}(z - z_1)/\sqrt{8\pi a_{ch}^3}, \qquad (18)$$

where $z_1 \sim z_0$ is a constant allowing the most accurate comparison of this approximation with the numerical solution of Eqs. (7a)–(7d). Using (17), we can readily determine the characteristic length Δz_{ch} at which the transverse size $a(z)$ reaches the stationary value a_{ch} at the final stage of the process under study. For initially broad beams with $a_0 \gg 1$, this length is proportional to the power $\mathcal{P}$ and is

$$\Delta z_{ch} = \mathcal{P}/(8\sqrt{2\pi}\cos^2\gamma_0). \qquad (19)$$

A comparison between (16) and (19) shows that z_0 considerably exceeds Δz_{ch}. Thus, for $\mathcal{P} > \mathcal{P}_{cr1}(a_0)$, the evolution of the wave field (in the absence of radiative losses) includes two stages: at the first stage, the main self-focusing of radiation occurs, and, at the final stage, a waveguide channel is formed. Note that the second stage is considerably shorter than the first one. According to (18), as the effective width $a(z)$ decreases down to the minimal size a_{cr}, the phase-front curvature $\beta(z)$ increases linearly with increasing z along the beam propagation path in contrast to the usual self-channeling regime. This scenario most likely corresponds to a collapse resulting in the formation of a nonlinear wave structure with a finite width.

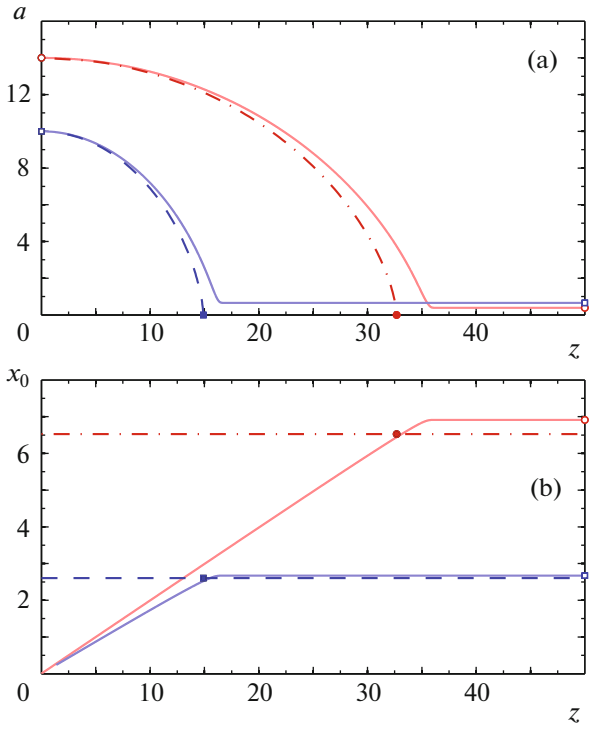

Fig. 1. (Color online) Transverse size $a(z)$ and position $x_0(z)$ of the peak intensity of the initially collimated wave beam with the initial width a_0 and linear phase-front correction γ_0 for power $\mathcal{P} > \mathcal{P}_{cr1}(a_0, \gamma_0)$. Solid curves are obtained from Eqs. (7a)–(7d) for $a_0 = 10$, $\gamma_0 = 0.0875$, $\mathcal{P} = 6.9917$ (lines with light squares) and $a_0 = 14$, $\gamma_0 = 0.1$, $\mathcal{P} = 3.9953$ (lines with light circles). In Fig. 1a, approximation (15) for the function $a(z)$ and the self-focusing length z_0 determined from (16) are shown for the first combination of a_0, γ_0, and $\mathcal{P}$ by the dashed curve and square, respectively, and for the second combination of a_0, γ_0, and $\mathcal{P}$ by the dot-and-dash line and circles, respectively. In (b), the estimate (21) of the finite displacement Δx_0 of the maximum of the field amplitude across the array of optical fibers for $a_0 = 10$, $\gamma_0 = 0.0875$, and $\mathcal{P} = 6.9917$ is shown by the dashed line and for $a_0 = 14$, $\gamma_0 = 0.1$, and $\mathcal{P} = 3.9953$ – by the dot-and dash straight line.

The one-dimensional collapse of the wave field resulting in radiation localization at scales comparable with the period of an array of equidistant optical fibers substantially affects all the aspects of the beam behavior in the spatially inhomogeneous medium considered here—in particular, the beam displacement across the array. In the aberrationless approximation, a change in the propagation direction can be easily observed. This leads to a considerable distortion in the motion path of the center of masses of the initially col-

limated broad beam coupled to a system of nonlinear optical waveguides at an angle to the axis directed along them, which converges to a channel during self-focusing.

The presence of the first integral (9) in the problem (7a), (7b) allows us to rewrite Eq. (7c) for the position $x_0(z)$ of the radiation intensity maximum in the form

$$\frac{dx_0}{dz} = 2\sin\gamma_0\left(\mathscr{C} - \frac{Q}{2a}\right). \tag{20}$$

It follows directly from (20) that in the absence of the wave-field self-channeling, i.e., for $\mathscr{P} \le \mathscr{P}'_{cr}$ ($Q \le Q'_{cr}$), the beam will constantly shift across the array of equidistant optical fibers with almost constant velocity, slightly decelerating with decreasing $a(z)$ and then slightly accelerating again with increasing $a(z)$. In other words, the beam propagates at an angle to the system axis whose value weakly oscillates with respect to the average value γ_0. In this case, the oscillation period coincides with the changing period of the effective width $a(z)$. A completely different picture can be observed in a situation when the field is captured in a channel with the transverse size a_{ch}. In this case, the right-hand side of relation (20) vanishes, which indicates to a considerable turn of the beam path and a cessation of its motion as a whole in the direction perpendicular to optical fibers. This peculiar "stop" effect appears due to localization of radiation in a region with the characteristic scale on the order of the distance between two neighboring nonlinear optical waveguides.

Let us estimate the displacement of the position $x_0(z)$ of the wave-field intensity maximum before the angle between the beam propagation direction and the z axis along which optical fibers are oriented will become zero. Assume that the derivative dx_0/dz remains constant and equal to $2\sin\gamma_0$ until radiation trapping in a channel for $z = z_*$ and then the coordinate x_0 ceases to change; i.e., $x_0(z > z_*) = x_0(z_*)$. This assumption is based on the results of calculations performed directly with the help of Eqs. (7a)–(7d) and also on the analysis presented above, which allows separating two different (short and long) stages of radiation self-focusing at powers $\mathscr{P}$ exceeding the critical value $\mathscr{P}_{cr1}(a_0, \gamma_0)$. In particular, Fig. 1b demonstrates dependences $x_0(z)$ typical for $\mathscr{P} > \mathscr{P}_{cr1}$ (a_0, γ_0) and confirming the possibility of using this approximation. In addition, using asymptotic relations (17) and (20) valid for $z \to \infty$, we can easily show that the characteristic distance on which the beam mainly changes its direction coincides with Δz_{ch} and is determined by expression (19). As z_*, with the same accuracy as in the previous assumption, we can take the self-focusing length z_0 calculated from (16). As a result, the final displacement Δx_0 of the beam with respect to its initial position is approximately

$$\Delta x_0 = 2z_0\sin\gamma_0 = \frac{\pi^{5/4}a_0^{3/2}\sin\gamma_0}{2^{3/4}\sqrt{\mathscr{P}\cos\gamma_0}}. \tag{21}$$

The estimate for Δx_0 coinciding with relation (21) can be also obtained for powers $\mathscr{P}$ not strongly exceeding $\mathscr{P}_{cr}$ using another, more formalized approach. First of all, based on Eqs. (7a) and (7c), we can easily see that the equality

$$\frac{dx_0}{da} = \frac{\tan\gamma_0}{2\beta a} \tag{22}$$

is valid in the aberrationless approximation. Then, we assume that conditions are fulfilled for which approximation (13) is valid for relation between the phase-front curvature $\beta(z)$ and the effective width $a(z)$ of the amplitude distribution. In particular, we will assume that for $z = 0$ (at the system input), a broad collimated beam is specified, i.e., $a(z = 0) = a_0 \gg 1$ and $\beta(z = 0) = 0$, and perform our analysis at the initial self-channeling stage when the value of $a(z)$ still remains large enough compared to the final transverse size a_{ch} of the channel. By substituting expression (13) instead of β into (22), we obtain the equation

$$\frac{dx_0}{da} = \pm\frac{\tan\gamma_0}{\sqrt{2Q}}\sqrt{\frac{a_0 a}{a_0 - a}}, \tag{23}$$

which can be easily integrated, as in the case with (14), to find the dependence $x_0(a)$ in the explicit form

$$x_0(a) = \pm\sqrt{\frac{a_0}{2Q}}\tan\gamma_0\left(-\sqrt{a(a_0 - a)} - a_0\left(\frac{\pi}{2} - \arcsin\sqrt{\frac{a}{a_0}}\right)\right). \tag{24}$$

To estimate the resulting displacement Δx_0 of the radiation intensity maximum during the wave-field self-focusing, we should substitute $a = a_{ch}$. However, when $a_{ch} \lesssim 1$, i.e., for $\mathscr{P}$ not strongly exceeding $\mathscr{P}_{cr}$, we can set a equal to zero, as in deriving expression (16) for the length z_0 beginning from which a one-dimensional collapse passes to the final channel-formation stage. As a result, with a slightly deteriorated accuracy, we obtain expression (21).

Figure 1b clearly demonstrates that relation (21) gives the adequate value of Δx_0 and can be used for analytic approximation. One can see that Δx_0 decreases inversely proportional to $\sqrt{\mathscr{P}}$. Therefore, the maximum displacement Δx_0 of the center of masses of the beam with respect to its initial position at the input to the system of equidistant optical fibers should be expected for the power $\mathscr{P}$ close to the critical power $\mathscr{P}_{cr1}(a_0, \gamma_0)$. In addition, by setting Δx_0 equal to the array period (i.e., to unity in dimensionless variables used), we can estimate another critical power

$$\mathcal{P}_{cr2}(a_0, \gamma_0) = \pi^{5/2} a_0^3 \sin^2 \gamma_0 / \sqrt{8} \cos \gamma_0, \quad (25)$$

above which the wave-field intensity maximum will not strongly shift in the transverse direction and the beam will initially propagate parallel to the axis oriented along nonlinear optical waveguides without any noticeable deviations. Note that $\mathcal{P}_{cr2}(a_0, \gamma_0)$ can be either greater or smaller than $\mathcal{P}_{cr1}(a_0, \gamma_0)$ depending on two parameters a_0 and γ_0. If $\mathcal{P}_{cr2}(a_0, \gamma_0) \le \mathcal{P}_{cr1}(a_0, \gamma_0)$, then the beam with $\mathcal{P} > \mathcal{P}_{cr1}(a_0, \gamma_0)$ coupled to the system at the angle γ_0 will be captured in the initially central optical fiber, i.e., the number of a structural element of the array with the peak field amplitude will not change. It also follows from this that, by equating $\mathcal{P}_{cr2}(a_0, \gamma_0)$ to the lower boundary $\mathcal{P}'_{cr}$ of the interval of possible values of $\mathcal{P}_{cr1}(a_0, \gamma_0)$, we will find the minimal angle

$$\gamma_0^{\min}(a_0) = \arctan\left(\frac{\sqrt{8Q'_{cr}}}{\pi a_0^{3/2}}\right) \approx \arctan\left(\frac{2.2592}{\pi a_0^{3/2}}\right), \quad (26)$$

for each specified size a_0 of the collimated beam beginning from which linear corrections of the field phase front become essential for self-channeling. For $|\gamma_0| \le \gamma_0^{\min}(a_0)$ and $\mathcal{P} > \mathcal{P}_{cr1}(a_0, \gamma_0)$, the transverse displacement of the beam will certainly be absent.

Thus, the analytic study shows that for powers $\mathcal{P}$ exceeding the critical value $\mathcal{P}_{cr1}$, the radiation self-channeling into a separated optical fiber occurs. This process changes the type of propagation of a wave beam coupled to a system of equidistant optical fibers at the angle γ_0 to the z axis oriented along them. "Above-critical" beams deviate from the initial linear propagation direction and are localized in a structural element displaced with respect to an optical fiber, which is initially central for a symmetric amplitude distribution. This deviation decreases with increasing $\mathcal{P}$. As a result, high-power inclined beams with $\mathcal{P} > \mathcal{P}_{cr2}$ and $\gamma_0 \neq 0$ should be captured into a channel without any visible displacements perpendicular to the z axis.

3. NUMERICAL SIMULATIUON OF RADIATION SELF-FOCUSING IN A DISCRETE SYSTEM

In this section, we discuss the results of detailed DNSE (1) numerical calculations of the spatial dynamics of initially collimated broad wave beams injected into an array of equidistant identical optical fibers at an angle to their orientation direction. The field distribution at the input to the system was specified in the form

$$\Psi_n(z = 0) = \sqrt{\frac{\mathcal{P}}{\sqrt{\pi} a_0}} \exp\left(-\frac{n^2}{2a_0^2} + i\gamma_0 n\right), \quad (27)$$

which corresponds to expression (5) with initial parameters $a(0) = a_0$, $x_0 = 0$, $\gamma(0) = \gamma_0$, and $\beta(0) = 0$.

The numerical DNSE simulation (1) demonstrates a more complex and rich picture of radiation evolution compared to that predicted by the analytic description developed in Section 2.1. Apart from the appearance of aberrations, this is caused by the following reasons. First, according to the inverse scattering problem for the NSE, the initially limited distribution gradually transforms to a set of mutually interaction solitons [1–3] from which, in particular, breathers are formed [1–3]. Therefore, as in the continual problem, within the framework of DNSE (1), an initially broad intense beam can stratify into several soliton-like structures, which violates the assumption about the single-scale nature of the test function describing the wave-field form. Second, the behavior of nonlinear formations in a discrete system is strongly affected by radiative losses, which are naturally present in DNSE (1) simulations and lead to emission of a part of radiation from the main region of its localization. Because of some factors neglected in the variational approach, along with aberrationless regimes, a number of effects are observed which strongly affect the spatial dynamics and self-channeling of beams. However, before proceeding to a detailed discussion of data obtained by direct numerical calculations of $\Psi_n(z)$, note that analysis presented in previous paragraphs considerably improves the understanding of composite processes proceeding in the system under study. In addition, our estimates are in good agreement with the values obtained by the numerical solution of DNSE (1).

Figures 2 and 3 present the results of the DNSE simulation of the self-focusing of initially Gaussian beams with the plane wave front (see (27)) in a periodic system of optical fibers for $\gamma_0 = 0.1$ and $a_0 = 7$ (Fig. 2) and $a_0 = 14$ (Fig. 3). Each fragment in these figures demonstrates one of the possible typical scenarios of the spatial dynamics of the wave field produced depending on the quantity $\mathcal{P}$. The data presented above describe quite completely the evolution of broad beams introduced at an angle to the z axis.

In Figs. 2a and 3a for $z = 0$, the radiation power $\mathcal{P} = 2.5$ is lower than the bifurcation value $\mathcal{P}'_{cr}$. One can see that the wave field propagates in this case on average along a straight line that does not coincide in the general case $\gamma_0 \neq 0$ with the z axis. This means that the coefficient γ responsible for the linear correction of the wave front remains almost constant and approximately equal to γ_0. Also, it is easy to see that the width of the amplitude distribution changes in fact periodically. The main part of the beam is periodically compressed down to a few periods of the array and then is expanded up to the initial size. Note especially that for

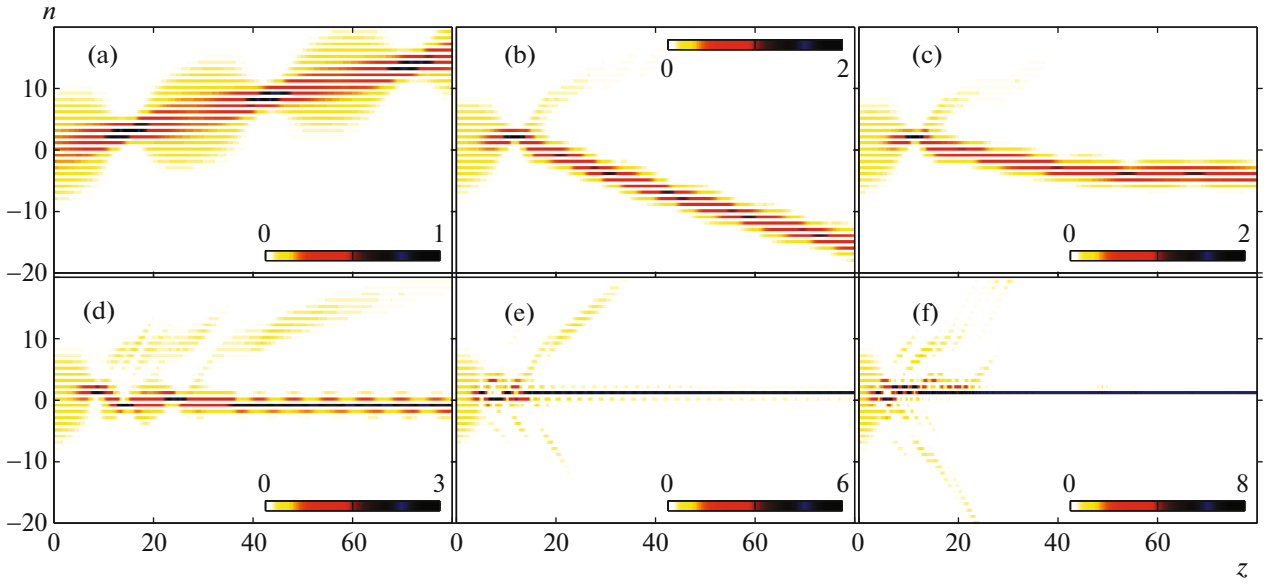

Fig. 2. (Color online) Spatial dynamics of the intensity $|\Psi_n(z)|^2$ of a wave beam calculated by direct numerical DNSE (1) simulation. The beam is specified for $z = 0$ by (27) with $a_0 = 7$, $\gamma_0 = 0.1$ and $\mathcal{P} = 2.5$ (a), 3.25 (b), 3.5 (c), 4.5 (d), 9 (e), and 15 (f).

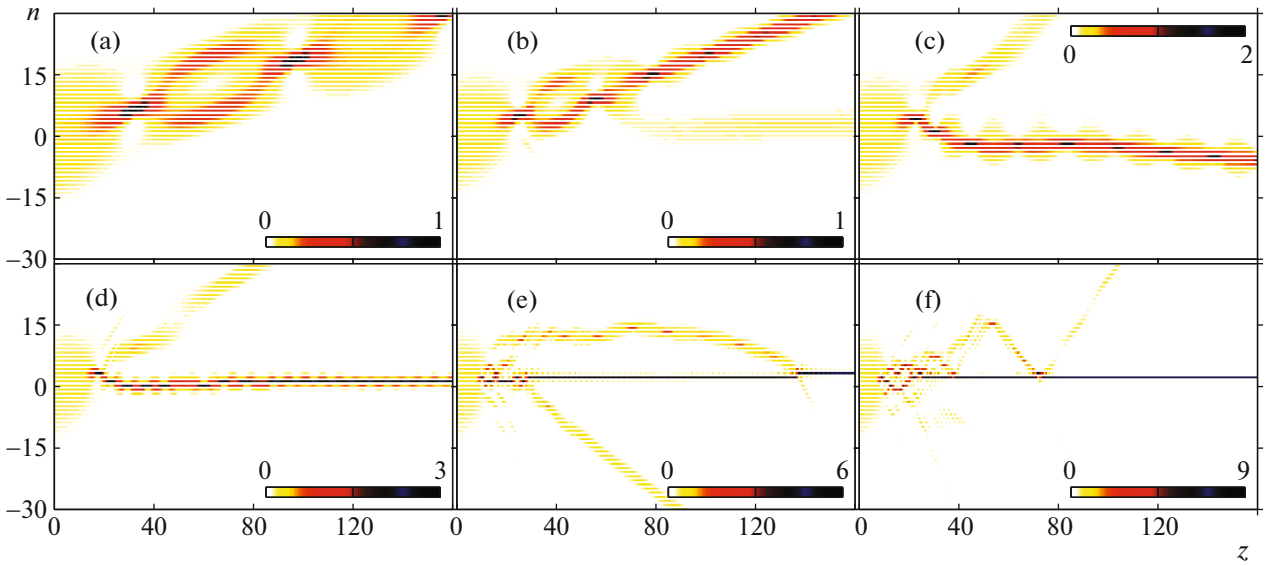

Fig. 3. (Color online) Same as in Fig. 2, but for $a_0 = 14$ and $\mathcal{P} = 2.5$ (a), 3.5 (b), 4 (c), 5.5 (d), 13 (e), and 17 (f).

parameters of numerical calculations corresponding to Figs. 2a and 3a, the effective width never becomes smaller than the distance between neighboring optical fibers and no radiation trapping in a channel is observed. Such a behavior qualitatively coincides with theoretical concepts based on the analysis of possible solutions of the system of ordinary differential equations (7a)–(7d) and developed in Section 2. Note, however, two important moments. Although $\mathcal{P} < \mathcal{P}'_{cr}$, radiative losses are relatively weak, they increase with approaching $\mathcal{P}$ to $\mathcal{P}'_{cr}$. Figure 3a shows that the beam decompose during its propagation into several components. In fact, such effects appear in this situation due to the closeness to the continual limit.

When the initial radiation power $\mathcal{P}$ weakly differs from the first bifurcation value $\mathcal{P}'_{cr}$ at which the phase plane of the conservative system of equations (7a), (7d) undergoes topological modifications, the spatial dynamics of wave beams in a discrete array of optical

fibers also begins to change strongly. This is clearly demonstrated in Fig. 2b presenting the results of numerical DNSE simulations (1) for the wave field specified for $z = 0$ in form (27) with $\mathcal{P} = 3.25$, $a_0 = 7$ and $\gamma_0 = 0.1$. For such parameters, the input radiation power $\mathcal{P} = 3.25$ slightly exceeds $\mathcal{P}'_{cr} \approx 3.18336$. One can see that the initially broad beam propagates at the initial stage along a straight line and is compressed down to the period of the structural medium under study. During the beam compression, the radiation intensity maximum in the beam cross section increases and achieves its maximal value when almost all the field is collected in one optical fiber. The processing of numerical calculation data shows that the main parameters of the beam (first of all, its effective width $a(z)$ and the position $x_0(z)$ of the center of masses) drastically change at the final stage of the process, which is qualitatively consistent with the theoretical analysis and estimates presented in Section 2.2. As a result, large radiative losses appear, which are seen in Fig. 2b. They cause cardinal changes in the wave-field evolution. Later on the preserved beam ceases to shift along the previous direction, as in the situation shown in Fig. 2a. The motion path of the amplitude distribution maximum is considerably distorted; i.e., the angle of propagation of the main part of radiation with respect to the z axis noticeably changes. It even appears visually that the beam is reflected from a cell in which the wave field was focused (see, for example, Figs. 2b, 2c and 3c). As for the effective width, its oscillations become less noticeable or are in fact absent at all. This suggests the formation of a soliton-like structure due to radiative losses. Note, however, that the propagation paths of such wave structures localized on a small number of optical fibers can be both almost straight and strongly bent.

With increasing the input radiation power $\mathcal{P}$ in the system, once the initially broad beam is compressed down to the size of one waveguide and loses a fraction of its energy, the formation of channels discussed in Section 2 begins. For example, Fig. 2c shows that the focused beam turns through a smaller angle and the wave field remaining localized tends to propagate parallel to the direction along which structural elements of the inhomogeneous medium are oriented. The motion path of the intensity maximum deviates hither and thither from the z axis. This is probably explained by the fact that the power of the preserved nonlinear structure gradually increases and approaches the threshold $\mathcal{P}_{cr1}(a_0, \gamma_0)$ above which, according to the generalized aberrationless approximation, the radiation self-channeling should occur (see Section 2.2 and Appendix B). Note that this circumstance is caused not only by the increase in the power $\mathcal{P}$ of the beam injected at $z = 0$, but also by the increase in the length Δz_{ch} of the region where the behavior of the wave field drastically changes. Because it is the break of the adiabatic approximation for the evolution of the main parameters of the beam that most likely gives rise to strong radiative losses at the first collapse stage, a decrease in these losses should be reasonably expected with increasing Δz_{ch}.

According to numerical DNSE (1) calculations, the formation of a channel at the array-period scale from initially broad beams and the concentration of a greater part of radiation in one of the optical fibers occur only for $\mathcal{P} > \mathcal{P}_{cr}$. An example is presented in Fig. 2d corresponding to the power $\mathcal{P} = 4.5$ weakly exceeding the bifurcation value $\mathcal{P}_{cr} \approx 4.2787$. This figure shows how a long enough transient process, nevertheless, ends the self-channeling of the wave field concentrating in a region of size on the order of the distance between neighboring structural elements of the chain under study and then propagating exactly along the z axis.

The tendencies and behavior described above are also observed in simulations of the spatial dynamics of initially collimated beams specified for $z = 0$ in form (27) with $a_0 = 14$ and $\gamma_0 = 0.1$. In particular, Figure 3b shows that the wave field for $\mathcal{P} = 3.5$ is compressed down to the array-period scale, which is accompanied by strong radiative losses. However, in this case, the wave field stratifies after collapse into two nonlinear structures with different powers. One of them gradually diffracts, while another exhibits a few oscillations of its width, thereby losing a part of its energy, and then transforms to a soliton-like structure concentrated on several waveguide elements, still displacing across the z axis. Note that here no sharp and strong distortion of the motion path of the localized part of the beam is observer; i.e., the propagation direction changes not so strongly as, for example, in situations in Figs. 2b, 2c. Note also that it seems that the splitting into nonlinear structures described above is inseparably related to the prerequisites of passing from the initial Gaussian amplitude distribution to the wave field which alternately decomposes into two interacting components and is gathered to one (see Fig. 3a). This, in particular, causes a strong energy loss, which can amount to 30% of the initial radiation power $\mathcal{P}$.

As $\mathcal{P}$ approaches $\mathcal{P}_{cr} \approx 4.2787$ for a beam with $a_0 = 14$, the relative radiative losses decrease; however, they remain large in magnitude. As a result, the nonlinear structure is dropped and its transverse sizes oscillate during its further spatial dynamics. Because of the recoil, the angle at which the remaining part of the wave field propagates with respect to the z axis noticeably changes. Thus, we can say that the reflection of the beam is observed again from the point of compression, as in the case $a_0 = 7$. An example for $\mathcal{P} = 4$ is presented in Fig. 3c. This figure also shows the tendency to the formation of a channel. However, the radiation self-channeling occurs only for $\mathcal{P} > \mathcal{P}_{cr} \approx 4.2787$ due to the additional long enough transient process, as illustrated in Fig. 3d.

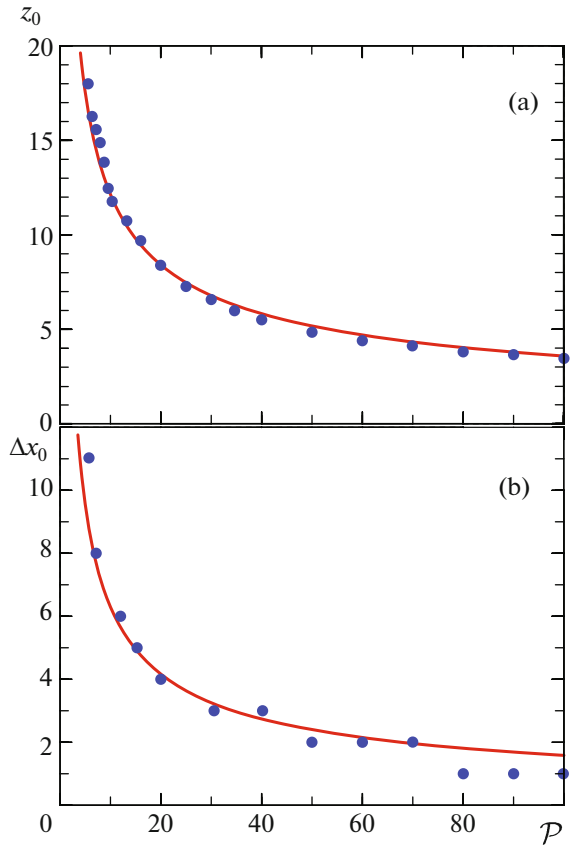

Fig. 4. (Color online) Self-focusing length z_0 and finite displacement Δx_0 of a point with the peak intensity across a discrete array as functions of the input power $\mathcal{P}$. Blue circles present the results obtained after processing data of the direct numerical DNSE (1) simulation. Solid curves show approximate analytic functions describing the dependences of (a) z_0 and (b) Δx_0 on $\mathcal{P}$ (taking into account the additional correction factor equal to 0.62 in this case). The plots correspond to $a_0 = 14$ and $\gamma_0 = 0.3$.

As $\mathcal{P}$ is increased, the region in which the beam is initially compressed down to the size smaller than the array period decreases. Also, the intermediate region decreases, which precedes the final concentration of a greater part of radiation in one of the nonlinear optical fibers and is characterized by main radiative losses. According to DNSE (1) calculations, the number of an optical fiber in which the light field was captured, most often coincides with the position of the intensity maximum at the first compression. In particular, this circumstance is clearly confirmed by Figs. 2e and 3f. Note especially that, when $\mathcal{P}_{cr}$ is considerably exceeded, nonlinear structures with powers sufficient for passing to the strong compression regime are dropped during radiative processes. As a result, a part of dropped radiation again returns to the formed channel and collides with it. Such spatial dynamics can be observed in Figs. 2f and 3e, 3f. In a number of situations, these collisions can cause the displacement of the final position of the maximum field value by one cell, as in Fig. 3e. In other cases (see, for example, Fig. 3f), radiation captured in the channel transfers into an adjacent optical fiber only on a small finite length of the propagation path, and then the field maximum returns back.

As a whole, the numerical DNSE (1) simulation gives a picture predicted in many respects by data obtained in the aberrationless approximation. A key role in this picture belongs to the self-focusing of radiation propagating at an angle to the z axis along which the periodic system of optical fibers is oriented. When the radiation power exceeds the critical value $\mathcal{P}_{cr}$, the wave field is captured in one of the optical fibers and the position of the amplitude-distribution maximum drastically deviates from the initial propagation direction. Despite the complex spatial dynamics of the beam, finally two experimentally observed characteristics can be separated: the self-focusing length z_0 and the displacement Δx_0 of a point with the peak intensity across the array. In the aberrationless approximation, these quantities are calculated approximately from corresponding analytic expressions (16) and (21). The values of z_0 and Δx_0 were numerically determined at the moment when the diameter of the initially broad beam became smaller than the discrete-array period. The comparison of estimates made from (16) and (21) with direct DNSE (1) calculations demonstrates quite good agreement taking into account an additional correction factor, which is common for $z_0(\mathcal{P})$ and $\Delta x_0(\mathcal{P})$ for the same a_0 and γ_0, although depends on the input beam parameters. Figure 4 demonstrates the dependences of z_0 and Δx_0 on the power $\mathcal{P}$ of radiation specified for $z = 0$ by (27) with $a_0 = 14$ and $\gamma_0 = 0.3$. Note first of all that the decrease in the self-focusing length z_0 and the displacement Δx_0 of the point with the peak intensity with increasing $\mathcal{P}$ are described by the laws close to $1/\sqrt{\mathcal{P}}$. This suggests that approximation (5) and the variational approach developed in Section 2 quite adequately describe the beam structure in the prefocal region.

The conclusions made above qualitatively explain experimental studies of the radiation propagation at an angle to the axis of a periodic system of optical fibers [25–29] and also can promote a deeper investigation of the features of the self-action of wave fields in discrete lattices.

4. CONCLUSIONS

Based on DNSE (1), we have studied in detail the self-focusing of wave beams injected at an angle to the axis of a system consisting of a set of equidistant identical optical fibers. We have proposed the analytic method describing the evolution of initially broad (at the scale of the structured medium under study) local-

ized field distributions in discrete lattices. Using power $\mathcal{P}$ as a controlling parameter, radiation self-action regimes are classified. The presence of three characteristic values $\mathcal{P}$, $\mathcal{P}'_{cr}$, $\mathcal{P}_{cr}$, and $\mathcal{P}_{cr2}$ is demonstrated. For $\mathcal{P} < \mathcal{P}'_{cr}$, the discreteness of the medium is weakly manifested and the spatial evolution of the wave beam occurs, in fact, as in a continuous medium (the intensity peak moves along a straight line, the width of the wave beam periodically changes, etc.). For $\mathcal{P} > \mathcal{P}'_{cr}$, the radiation self-channeling in one of the optical fibers becomes dominant and the beam path is strongly distorted. The numerical DNSE simulation of the problem shows that radiation capturing in an optical fiber is accompanied by strong radiative losses. They substantially affect the wave-field evolution behind the focal plane. In particular, beams with the initial power $\mathcal{P}$ lying in the interval $\mathcal{P}'_{cr} < \mathcal{P} < \mathcal{P}_{cr}$ are transversely reflected from a cell in which the wield was focused. For $\mathcal{P}$ considerably exceeding $\mathcal{P}_{cr}$, radiative losses lead to the formation of an intermediate region before the capturing of a greater part of radiation followed by its self-channeling in one of the nonlinear optical fibers. For $\mathcal{P} > \mathcal{P}_{cr2}$, the wave beam incident obliquely on an array of optical fibers is refracted at the interface and then propagates along the system axis. The deviation of the wave-beam intensity peak from the propagation direction considered in the paper is a new nonlinear effect reflecting specific features of a discrete system.

ACKNOWLEDGMENTS

The authors thank A.A. Balakin for useful discussions. The analytic description of the spatial evolution of the wave beam in the array of optical fibers (Section 2, Appendices A and B) was supported by the Russian Science Foundation (project no. 16-12-10472). The numerical DNSE simulation and interpretation of the calculation results (Section 3) were supported by the Russian Science Foundation (project no. 14-12-00811).

APPENDIX A

Consider in more detail the variational approach used in Section 2.1 for describing the propagation of wave beams in an array of equidistant optical fibers. As before, we substitute approximation (5) for $\Psi(z, x)$ into expression (4) for the Lagrange function $\mathcal{L}$ of initial model (1). However, now we will calculate the averaged Lagrangian $\overline{\mathcal{L}}$ taking into account terms with $n = 0$ and ± 1. For beams with the transverse size $a \gg \sqrt{2}/\pi$, the quantity $\exp(-\pi^2 a^2/2)$ can be treated as a small parameter μ of the problem. As a result, retaining only terms of the zero and first order of smallness in μ, we obtain

$$\overline{\mathcal{L}} = \frac{\mathcal{P}a^2}{2}\frac{d\beta}{dz} - \mathcal{P}\gamma\frac{dx_0}{dz} - 2\mathcal{P}\cos\gamma \times\exp\left(-\frac{1}{4a^2} - \beta^2 a^2\right) - \frac{\mathcal{P}^2}{\sqrt{8\pi}a} - \frac{\mathcal{P}^2}{\sqrt{2\pi}a} \times\exp\left(-\frac{\pi^2 a^2}{2}\right)\cos(2\pi x_0). \quad (A.1)$$

Euler equations for collective coordinates $a(z)$, $\beta(z)$, $x_0(z)$, and $\gamma(z)$ corresponding to $\overline{\mathcal{L}}$ (A.1) have the form

$$\frac{da}{dz} = 4\beta a\cos\gamma\exp\left(-\frac{1}{4a^2} - \beta^2 a^2\right), \quad (A.2a)$$

$$\frac{d\beta}{dz} = \cos\gamma\left(\frac{1}{a^4} - 4\beta^2\right)\exp\left(-\frac{1}{4a^2} - \beta^2 a^2\right) - \frac{\mathcal{P}}{\sqrt{8\pi}a^3} - \frac{\mathcal{P}(1+\pi^2 a^2)}{\sqrt{2\pi}a^3}\exp\left(-\frac{\pi^2 a^2}{2}\right) \times\cos(2\pi x_0), \quad (A.2b)$$

$$\frac{dx_0}{dz} = 2\sin\gamma\exp\left(-\frac{1}{4a^2} - \beta^2 a^2\right), \quad (A.2c)$$

$$\frac{d\gamma}{dz} = -\frac{\sqrt{2\pi}\mathcal{P}}{a}\exp\left(-\frac{\pi^2 a^2}{2}\right)\sin(2\pi x_0). \quad (A.2d)$$

The main changes here concern the second and fourth relations. In particular, according to (A.2c), the coefficient γ is no longer constant even in the aberrationless approximation. Note, however, that additional terms appeared in (A.2b) and (A.2c) are proportional to $\exp(-\pi^2 a^2/2)$, i.e., to a small parameter μ. Therefore, their contribution to the dynamics of system (A.2a)–(A.2d) is often insignificant even for localized wave fields with the effective width a comparable with the array scale. Nevertheless, these corrections can affect the long-term evolution of relatively narrow beams. For example, it follows from (A.2a)–(A.2d) that stationary field distributions with a constant finite width are possible only at zero linear and quadratic corrections of the phase front. In addition, the condition $\sin(2\pi x_0) = 0$ should be also fulfilled, which is valid when $x_0 = m$ or $x_0 = m + 1/2$, where m is an integer. Here, we see the correspondence with two well-known soliton solutions of DNSE (1), one of which is stable ($x_0 = m$), while another is unstable ($x_0 = m + 1/2$) (see, for example, [3–9]).

The physical interpretation of effects caused by additional terms with $n = \pm 1$ in (4) considered in the calculation of the averaged Lagrangian $\overline{\mathcal{L}}$ can be obtained by comparing expressions (6) and (A.1). It is easy to see that the difference is only in one term containing a periodic function of the position x_0 of the radiation intensity maximum and representing the so-called Peierls–Nabarro (PN) potential [3–9]. This potential was first discussed in the theory of crystal dislocations (see details in [9]). However, it was shown

later that its existence principally affects the motion of kinks and solitons in various discrete models and, as a result, the behavior of solitary wave structures in arrays of coupled elements differs from their evolution in a continuous medium [3–9].

The authors of papers [10, 35] proposed to calculate the shape of the PN potential for DNSE (1) by the method using the closeness of (1) to the exactly integrable Ablowits–Ladik (AL) model [2, 4, 9]. The perturbation theory [10, 35] based on the inverse scattering transformation, in which differences of DNSE (1) from the system of AL equations are considered as small corrections, describes the dynamics of a broad soliton based on self-consistent ordinary equations for the coordinate of the center of mass and the linear correction coefficient in the phase. In this case, the transverse size of an exciton proves to be invariable in the approximation considered in [10, 35]. A comparison of relations (A.2c) and (A.2d) with relations obtained in [10, 35] for analogous quantities shows that their structures are very similar. In particular, if the effective width a of the amplitude distribution is assumed finite and virtually constant and the phase-front curvature β is assumed close to zero, then, according to (A.2c) and (A.2d), the evolution of parameters x_0 and γ of such a soliton-like wave beam will occur under the action of a periodic potential. As in [10, 35], the amplitude of this potential decreases exponentially with increasing a. Note that a nonlinear localized structure in DNSE (1) can be captured near one of the minima of the PN potential relief [10, 35]. However, the stop of the beam displacement across the array of optical fibers has a different physical nature and is caused first of all by the collapse of the wave field, although the PN potential, of course, favors the radiation self-channeling and leads to additional radiative losses during the spatial dynamics of the beam.

APPENDIX B

According to analysis presented above, the behavior of the dynamic system described by Eqs. (7a) and (7b) considerably depends on the range from $Q \le Q'_{cr}$, $Q'_{cr} < Q < Q_{cr}$, or $Q \ge Q_{cr}$ where the positive parameter Q lies. Before specifying the bifurcation values Q'_{cr} and Q_{cr}, we will illustrate qualitative transformations proceeding in the general picture of possible regimes of "motions" of such a system when Q passes through points Q'_{cr} and Q_{cr}.

Figure 5a shows the a_0, Q plane (a_0 is the effective width of a collimated wave beam) in which regions $Q \le Q'_{cr}$, $Q'_{cr} < Q < Q_{cr}$ and $Q \ge Q_{cr}$ are indicated with three different colors different from each other not only in color, but also in contrast. The characteristic phase portraits of the autonomous system of ordinary differential equations (7a), (7b) corresponding to these regions are presented in Figs. 5b, 5c, 5d. For Fig. 5a $Q = 0.45 < Q'_{cr}$. In this case, there exist two equilibrium states: the saddle A' (red square) and the center C' (blue circle). Note especially that for $Q < Q'_{cr}$, separatrices (in Fig. 5b, red curves beginning or ending at the saddle point A') are unclosed lines. Therefore, when $Q < Q'_{cr}$, there exists a specific phase trajectory in the two-dimensional phase space a, β separating the regions of infinite and finite motions. This trajectory intersects the $\beta = 0$ axis for a finite effective width a and then for $a \to +\infty$. Such a curve in Fig. 5b is shown by a green line passing through the point B' (green rhomb). For $Q = Q'_{cr}$, the parts of the phase trajectory described above symmetrically located with respect to the straight line $\beta = 0$ coincide with the corresponding separatrices, which in turn are closed for $a \to +\infty$, thereby producing prerequisites for generating a loop. When the parameter Q lies in the interval $Q'_{cr} < Q < Q_{cr}$, Eqs. (7a), (7b) have a doubly asymptotic solution separating now the flight and captured motion regimes of the system under study, which is clearly demonstrated for $Q = 0.675$ in Fig. 5c. The separatrix loop (red curve) in this figure starting (for $z \to -\infty$) from the saddle A (red square) and returning (for $z \to +\infty$) to it, makes a coil around the equilibrium state of the center C type (blue circle) turning at the point B (red rhomb) with coordinates $a \approx 7.517$, $\beta = 0$. The phase trajectories lying inside the loop describe oscillations of the effective width $a(\zeta)$ and the wave-front curvature $\beta(\zeta)$ of a Gaussian wave beam. If the initial parameters of radiation are such that the imaging point on the α, β phase plane lies initially in the external region for the separatrix, then the field will finally be localized in the approximation used in one of the optical fibers of the equidistant array. For $Q = Q_{cr}$, the saddler and center merge. As a result, when $Q > Q_{cr}$, the equilibrium states of the autonomous system of equations (7a), (7b) disappear and the phase space a, β becomes topologically simpler, which is seen, for example, in Fig. 5d constructed for $Q = 0.9$. In this case, the variational analysis predicts that any beam should be captured in a channel.

The equilibrium states of the system (7a), (7b) exist only for $\beta = 0$; i.e., for a plane phase front, while the effective width a_0 of such stationary beams is related to Q by the expression

$$\exp\left(-\frac{1}{4a_0^2}\right) = Qa_0. \qquad \text{(B.1)}$$

Transcendental Eq. (B.1) has two solutions $a_{0(1)}(Q)$ and $a_{0(2)}(Q)$ corresponding to the saddle and center on the a, β plane only for $Q < \sqrt{2/e}$. This is, in particular, clearly demonstrated in Fig. 5a, where the dotted red line passing through points A' and A (red squares) and the dashed blue line passing through points C' and C (blue circles) show dependences $Q(a_{0(1)})$ and $Q(a_{0(2)})$ corresponding to these equilibrium states. Thus, the

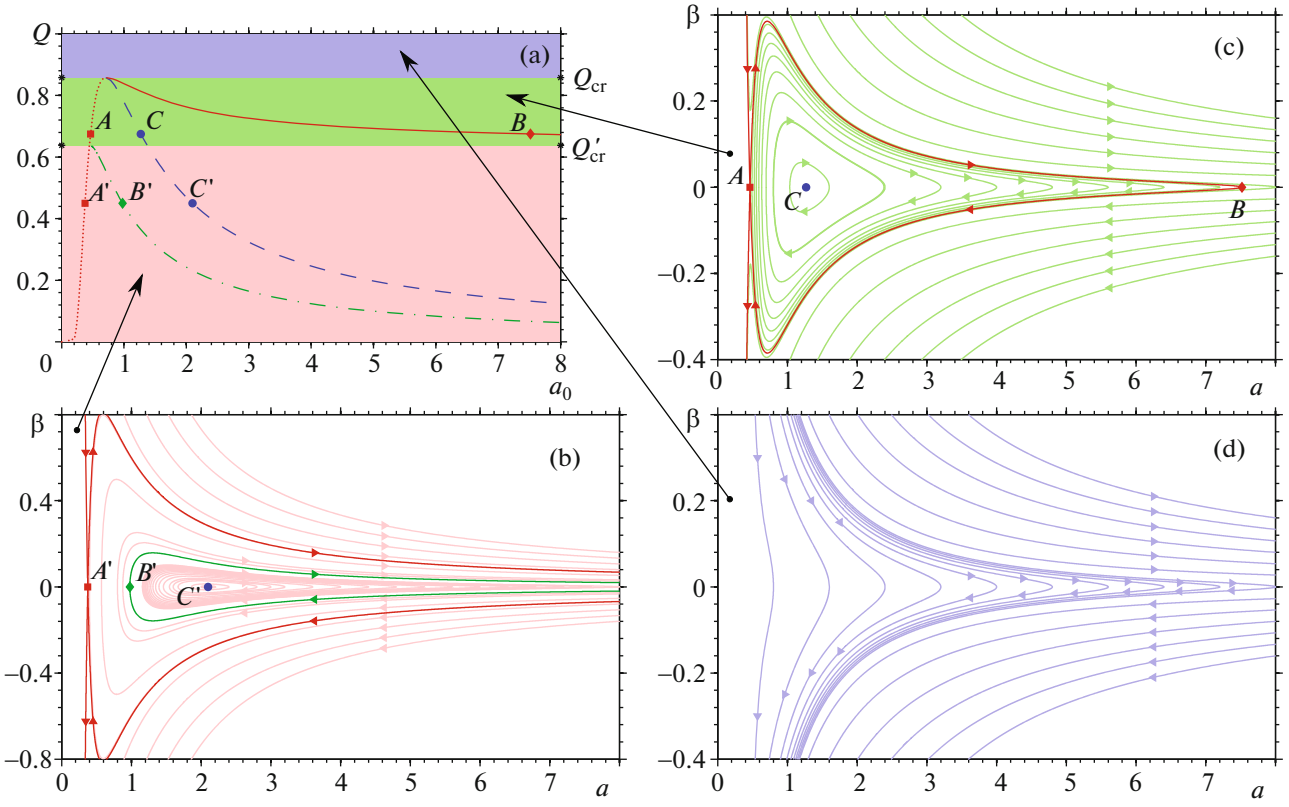

Fig. 5. (Color online) (a) The (a_0, Q) plane in which regions with qualitatively different behavior of the dynamic system (7a), (7b) are distinguished. Dependences $Q(a_0)$ for the equilibrium states of the system are shown by the dotted curve (saddle) and the dashed curve (center). The dot-and-dash curve shows the function $Q(a_0)$ determining in the (a, β) phase space the position of the point $a = a_0$, $\beta_0 = 0$ lying on the trajectory separating the regions of infinite and finite motions for $Q \le Q'_{cr}$. The solid curve specifies the effective width a_0 of the beam at the turning point of the separatrix loop for different values of Q in the interval $Q'_{cr} < Q \le Q_{cr}$. Figures (b, c, d) demonstrate topologically different (a, β) phase planes constructed for $Q = 0.45 < Q'_{cr}$, $Q'_{cr} < Q = 0.675 < Q_{cr}$, and $Q = 0.9 > Q_{cr}$. Squares in (b, c) indicate saddles A' and A and circles – centers C' and C. In (b), the line passing through the pony B' (rhomb) corresponds to the trajectory separating regions of the flight and captured behavior. Figure (c) is characterized by the presence of the separatrix loop coming out from the saddle A and returning to it after turning at the point B (rhomb).

bifurcation value of Q_{cr} is determined from the condition of the presence of the only solution of (B.1) and is equal to $Q_{cr} = \sqrt{2/e} \approx 0.8578$.

Taking into account integral (9), we see that, if for $Q < Q'_{cr}$, the transverse size $a_{0(3)}$ of a collimated wave beam satisfies the expression

$$\exp\left(-\frac{1}{4a_0^2}\right) + \frac{Q}{2a_0} = 1, \qquad \text{(B.2)}$$

then the point with coordinates $a_{0(3)}$, $\beta = 0$ in the a, β phase space lies on the trajectory separate by us earlier, which is closed at infinity and separates the regions of infinite and finite motions. The plot of the function $Q(a_{0(3)})$ obtained using (B.2) is shown in Fig. 5a by the dot-and-dash green curve containing also the point B' (green rhomb) corresponding to the point B' in Fig. 5b. One can see from Fig. 5a that the bifurcation value Q'_{cr} is determined by the intersection of the dotted and dot-and-dash curves, i.e., by the combined solution of Eqs. (B.1) and (B.2). As a result, we have finally $Q'_{cr} \approx 0.6382$.

Apart from three curves described above, another red solid curve presented in Fig. 5a, which is completely located in the region with $Q'_{cr} < Q < Q_{cr}$. It determines the effective width $a_{0(4)}(Q)$ at the turning point of the separatrix loop depending on the parameter Q from the interval $Q'_{cr} < Q \le Q_{cr}$. In this case, if the wave beam with the zero phase-front curvature has the transverse size a_0 for which the point a_0, Q proves to be below the given solid curve $Q(a_{0(4)})$, then, according to the above discussion, the periodic variations of $a(\zeta)$ and $\beta(\zeta)$ should be observed. In the opposite case, radiation will be self-channeled, result-

ing in the field localization at the scale of one nonlinear optical waveguide. To find the dependence $Q(a_{0(4)})$, it is necessary first, by fixing Q, to find for equation (B.1) the smallest root $a_{0(1)}(Q)$ corresponding to the saddle equilibrium state. Then, by substituting $a = a_{0(1)}(Q)$ and $\beta = 0$ into (9), to calculate the first integral $\mathscr{C}$ on the separatrix and, using the specified Q and $\mathscr{C}$, to solve the equation

$$\exp\left(-\frac{1}{4a_0^2}\right) + \frac{Q}{2a_0} = \mathscr{C} \qquad \text{(B.3)}$$

for a_0 and to find the solution $a_{0(4)}(Q)$ different from $a_{0(1)}(Q)$. By repeating this procedure for different Q satisfying $Q'_{\mathrm{cr}} < Q \le Q_{\mathrm{cr}}$, we can easily reconstruct the function $Q(a_{0(4)})$.

REFERENCES

1. E. Infeld and G. Rowlands, *Nonlinear Waves, Solitons and Chaos* (Cambridge Univ. Press, Cambridge, 2000; Fizmatlit, Moscow, 2005).
2. A. Scott, *Nonlinear Science: Emergence and Dynamics of Coherent Structures* (Oxford Univ. Press, 1999; Fizmatlit, Moscow, 2007).
3. Yu. S. Kivshar and G. P. Agrawal, *Optical Solitons: From Fibers to Photonic Crystals* (Academic, San Diego, CA, 2003; Fizmatgiz, Moscow, 2005).
4. P. G. Kevrekidis, *The Discrete Nonlinear Schrödinger Equation: Mathematical Analysis, Numerical Computations and Physical Perspectives* (Springer, Berlin, 2009).
5. *Nonlinearities in Periodic Structures and Metamaterials*, Ed. by C. Denz, S. Flach, and Yu. S. Kivshar (Springer, Heidelberg, 2010).
6. P. G. Kevrekidis, K. O. Rasmussen, and A. R. Bishop, Int. J. Mod. Phys. B **15**, 2833 (2001).
7. F. Lederer, G. I. Stegeman, D. N. Christodoulides, G. Assanto, M. Segev, and Ya. Silberberg, Phys. Rep. **463**, 1 (2008).
8. Ya. V. Kartashov, B. A. Malomed, and L. Torner, Rev. Mod. Phys. **83**, 247 (2011); Rev. Mod. Phys. **83**, 405(E) (2011).
9. O. M. Braun and Yu. S. Kivshar, *The Frenkel-Kontorova Model: Concepts, Methods, and Applications* (Springer, Berlin, 2004; Fizmatlit, Moscow, 2008).
10. A. B. Aceves, C. de Angelis, T. Peschel, R. Muschall, F. Lederer, S. Trillo, and S. Wabnitz, Phys. Rev. E **53**, 1172 (1996).
11. D. J. Kaup, Math. Comput. Simul. **69**, 322 (2005).
12. D. J. Kaup and T. K. Vogel, Phys. Lett. A **362**, 289 (2007).
13. J. Cuevas, G. James, P. G. Kevrekidis, B. A. Malomed, and B. Sánchez-Rey, J. Nonlin. Math. Phys. **15**, 124 (2008).
14. J. Cuevas, P. G. Kevrekidis, D. J. Frantzeskakis, and B. A. Malomed, Physica D **238**, 67 (2009).
15. C. Chong, R. Carretero-González, B. A. Malomed, and P. G. Kevrekidis, Physica D **238**, 126 (2009).
16. C. Chong, R. Carretero-González, B. A. Malomed, and P. G. Kevrekidis, Physica D **240**, 1205 (2011).
17. H. Susanto and P. C. Matthews, Phys. Rev. E **83**, 035201(R) (2011).
18. C. Chong, D. E. Pelinovsky, and G. Schneider, Physica D **241**, 115 (2012).
19. M. Syafwan, H. Susanto, S. M. Cox, and B. A. Malomed, J. Phys. A: Math. Theor. **45**, 075207 (2012).
20. A. Trombettoni and A. Smerzi, Phys. Rev. Lett. **86**, 2353 (2001).
21. A. A. Balakin, A. G. Litvak, V. A. Mironov, and S. A. Skobelev, Phys. Rev. A **94**, 063806 (2016).
22. U. Al Khawaja, S. M. Al-Marzougb, H. Bahloulib, Commun. Nonlin. Sci. Numer. Simul. **46**, 74 (2017).
23. I. L. Garanovich, S. Longhi, A. A. Sukhorukov, and Yu. S. Kivshar, Phys. Rep. **518**, 1 (2012).
24. D. N. Christodoulides, F. Lederer, and Y. Silberberg, Nature **424**, 817 (2003).
25. H. S. Eisenberg, Y. Silberberg, R. Morandotti, A. R. Boyd, and J. S. Aitchison, Phys. Rev. Lett. **81**, 3383 (1998).
26. R. Morandotti, U. Peschel, J. S. Aitchison, H. S. Eisenberg, and Y. Silberberg, Phys. Rev. Lett. **83**, 2726 (1999).
27. H. S. Eisenberg, R. Morandotti, Y. Silberberg, J. M. Arnold, G. Pennelli, and J. S. Aitchison, J. Opt. Soc. Am. B **19**, 2938 (2002).
28. U. Peschel, R. Morandotti, J. M. Arnold, J. S. Aitchison, H. S. Eisenberg, Y. Silberberg, Th. Pertsch, and F. Lederer, J. Opt. Soc. Am. B **19**, 2637 (2002).
29. D. Cheskis, S. Bar-Ad, R. Morandotti, J. S. Aitchison, H. S. Eisenberg, Y. Silberberg, and D. Ross, Phys. Rev. Lett. **91**, 223901 (2003).
30. O. Morsch and M. Oberthaler, Rev. Mod. Phys. **78**, 179 (2006).
31. Th. Anker, M. Albiez, R. Gati, S. Hunsmann, B. Eiermann, A. Trombettoni, and M. K. Oberthaler, Phys. Rev. Lett. **94**, 020403 (2005).
32. R. Franzosi, R. Livi, G. Oppo, and A. Politi, Nonlinearity **24**, R89 (2011).
33. H. Hennig and R. Fleischmann, Phys. Rev. A **87**, 033605 (2013).
34. H. Hennig, T. Neff, and R. Fleischmann, Phys. Rev. E **93**, 032219 (2016).
35. A. A. Vakhnenko and Yu. B. Gaididei, Sov. J. Theor. Math. Phys. **68**, 873 (1986).

Translated by M. Sapozhnikov